

Morphological and rheological properties of PET/clay nanocomposites

Abbas Ghanbari · Marie-Claude Heuzey ·
Pierre J. Carreau · Minh-Tan Ton-That

Received: 1 June 2012 / Revised: 19 November 2012 / Accepted: 28 November 2012 / Published online: 3 January 2013
© Springer-Verlag Berlin Heidelberg 2012

Abstract This work investigates the effects of clay chemistry and concentration on the morphology and rheology of polyethylene terephthalate (PET)/clay nanocomposites. The complex viscosity of the PET nanocomposites exhibited a more solid-like behavior, in contrast to the matrix that had a frequency-independent viscosity. In addition, at high frequencies where the behavior of the matrix should be dominant, a lower complex viscosity of the nanocomposites was observed due to PET degradation in the presence of the organoclays. The high-frequency data were used to estimate the matrix degradation using the Maron–Pierce equation. The apparent molecular weight of the PET matrix was found to decrease from 65 kg/mol for the neat PET to 30 kg/mol for a PET nanocomposite containing 8 wt% Cloisite® 30B. The apparent yield stress in the nanocomposites was determined using the Herschel–Bulkley model. Yield stress increased with the level of exfoliation and clay concentration, from ~0 to 166 Pa when the clay concentration increased from 2 to 8 wt%.

Keywords Polyethylene terephthalate · Nanocomposites · Organoclay · Rheology · Morphology

Introduction

Polymer/layered silicate nanocomposites have attracted remarkable scientific and technological interests due to significant improvement of material properties, at low clay loadings, in comparison with unfilled polymers or common micro composites. These notable changes include enhancements in mechanical properties, thermal stability, barrier, and flame-retardant properties (Gupta et al. 2009; Ray and Okamoto 2003).

To prepare polymer/layered silicate nanocomposites, three main approaches consist of solution blending, in situ polymerization, and melt blending. Melt blending is an environmental friendly method because there is no need for organic solvents. Besides, low cost and common industrial processing techniques such as extrusion can be used for the preparation of nanocomposites from a wide range of thermoplastic polymers. In addition, the high shear force in polymer processing equipments facilitates the dispersion of the nanoparticles in the molten polymer matrix. Therefore, melt blending is industrially a more viable method in comparison to other approaches (Pavlidou and Papaspyrides 2008; Ray and Okamoto 2003).

Wide-angle X-ray diffraction (WAXD), scanning electron microscopy (SEM), and transmission electron microscopy (TEM) are the most common techniques to characterize the nanocomposite morphology. WAXD is a convenient and rapid method to determine the gallery spacing of silicate layers for both pristine clays and organically modified clays and when polymer chains penetrate into the galleries. However, little information about the distribution of the silicate layers can be obtained by this method. On the other hand, although TEM provides direct visual information about the distribution of the silicate layers, it is a time-consuming and expensive technique which covers only a very small

A. Ghanbari · M.-C. Heuzey (✉) · P. J. Carreau
Center for Applied Research on Polymers and Composites
(CREPEC), Chemical Engineering Department,
Ecole Polytechnique de Montreal, PO Box 6079,
Stn Centre-Ville, Montreal, QC H3C 3A7, Canada
e-mail: marie-claude.heuzey@polymtl.ca

M.-T. Ton-That
Automotive Portfolio, National Research Council Canada,
75 Mortagne Blvd, Boucherville, QC J4B 6Y4, Canada

portion of the sample, with the possibility of microscale inhomogeneity. SEM is used to characterize the particle distribution at the micrometer scale and to assess the presence of large aggregates. In conjunction with the aforementioned techniques, rheology is employed as an indirect tool for the microstructure characterization of nanocomposites. The advantage of rheological methods is that they probe the bulk of nanocomposite materials on a significant volume of sample tested, which increases the reliability of the data. In addition, measurements are performed in the melt state, which can provide valuable information about the processability of the nanocomposites. Furthermore, the interactions between the nanoparticles and the matrix can also be detected and quantified. Finally, detailed information about molecular level changes in the structure (e.g., oxidation, degradation, cross-linking, etc.) can be obtained by employing rheometry (Pogodina et al. 2008; Galindo-Rosales et al. 2011; Bhattacharya et al. 2007; Gupta et al. 2009; Vermant et al. 2007).

A large number of rheological studies have been carried out to assess the state of clay dispersion in polymer matrices, especially thermoplastics (Nazockdast et al. 2008; Wu et al. 2005; Vermant et al. 2007; Eslami et al. 2010; Wang et al. 2011; Aubry et al. 2005; Manitiu et al. 2009; Ayer and Leonov 2004; Gahleitner et al. 2006; Lim and Park 2001; Mobuchon et al. 2007, 2009a, b). Large increases in viscoelastic properties, storage modulus, and complex viscosity, as well as a slower relaxation and a transition from liquid-like to solid-like behavior are the most significant findings of these studies. The appearance of a solid-like terminal plateau in the storage modulus of nanocomposites has been commonly attributed to the formation of a space-filling percolated network of individual clay platelets and/or intercalated tactoids acting like a weak solid (Pujari et al. 2011; Utracki and Lyngaae-Jorgensen 2002; Solomon et al. 2001; Ren et al. 2000; Ray and Bousmina 2005). Therefore, by destroying this interconnected network of clay particles (for example by pre-shearing), a remarkable reduction of viscoelastic properties is expected. Orientation of clay particles in the shear direction and a transition from solid-like behavior to liquid-like behavior has been observed by many researchers (Nazockdast et al. 2008; Wu et al. 2005; Dykes et al. 2012; Solomon et al. 2001). The presence of a percolation network is also inferred by the stress response upon start-up of steady shear. The stress overshoot observed in transient rheological response of nanocomposites depends on rest time duration and applied shear rate, and is attributed to both interaction between nanoparticles and the viscoelastic properties of the polymer matrix.

Polyethylene terephthalate (PET) is a semi-crystalline thermoplastic polymer widely used in soft drink bottles as well as both food and nonfood containers. PET is nontoxic

and shows high dimensional stability, high transparency, and good mechanical and thermal properties. Barrier properties of PET to oxygen should, however, be improved for some applications like packaging of oxygen-sensitive beverages such as soft drinks and beer. Incorporation of silicate nanolayers into a PET matrix has been shown to enhance the barrier properties of PET (Ghanbari et al. 2012; Ghasemi et al. 2011a, 2012; Xu et al. 2011; Frounchi and Dourbash 2009; Soon et al. 2009).

Several studies have been performed on PET/organoclay nanocomposites. It was observed that introducing a PET-ionomer as an exfoliating agent, which has a higher polarity than PET, improved the dispersion of clay particles and increased the viscoelastic properties of the nanocomposites (Ghanbari et al. 2012; Xu et al. 2011). In another study, it was demonstrated that contrary to thermally stable phosphonium and imidazolium modified clays, ammonium-modified Cloisite® 30B (C30B) exhibited good dispersion and distribution within a PET matrix (Ghasemi et al. 2011b). The incorporation of 3 wt% of C30B into PET led to a 27 % reduction in oxygen permeability (Ghasemi et al. 2011a). Sanchez-Solis et al. (2004) observed that the incorporation of 3 wt% silicate nanolayers in a PET matrix resulted in a 45 % enhancement of the Young's modulus.

Although several studies have been devoted to polymer/clay nanocomposites, the rheological behavior of PET/clay nanocomposites is not fully understood. For example, it has been observed that the incorporation of 2 wt% Nanomer® I.28E (N28E) and C30B in the PET matrix reduces the complex viscosity (Ghanbari et al. 2012; Xu et al. 2011). Scaffaro et al. (2011) prepared PET nanocomposites containing C30B and Cloisite® 15A (C15A) using a twin-screw extruder. They observed that the complex viscosity of the nanocomposites containing 3, 5, and 10 wt% of the organoclays was smaller than that of the neat PET at high frequencies. More severe degradation was observed for the nanocomposites containing C30B than those containing C15A.

In the present work, various clay particles (from unmodified synthetic clay to commercially available organoclays) at different concentrations (from 0 to 8 wt%) were used to study the effect of surfactant and clay concentration on the rheological properties of PET nanocomposites. In addition, by changing the twin-screw configuration, the effect of processing was also examined. To our knowledge, there is no work addressing the effects of these parameters on both the rheology and morphology of PET nanocomposites in order to have a more in-depth comprehension. Particular emphasis is placed on studying the yield stress of the solid-like network induced by the presence of the clay particles at clay concentrations higher than the percolation threshold. High-frequency data are used to estimate the thermal degradation

Table 1 Characteristics of the clay particles

Organoclay	Organic modifier	<i>d</i> -spacing (nm)	Organic modifier (wt%)	δ of organic modifier ^{a,b} ($\text{J}^{1/2} \cdot \text{cm}^{-3/2}$)
C30B	Methyl, tallow, bis-2-hydroxyethyl, quaternary ammonium	1.85	29	21.5
C25A	Dimethyl, dehydrogenated tallow, 2-ethylhexyl quaternary ammonium	1.86	31	17.2
N28E	Octadecyl ammonium	2.4	33	16.0
C15A	Dimethyl, dehydrogenated tallow, quaternary ammonium	3.15	40	16.9
SM100	none	0.96	0	–

^a δ is the solubility parameter calculated based on the Fedors group contribution method (Van Krevelen and Te Nijenhuis 2009)

^bExperimental value of δ for PET is between 19.9 and 21.9 (Van Krevelen and Te Nijenhuis 2009)

of the PET matrix and analyze the influence of clay content on a more solid basis. Rheological properties are also correlated with morphological observations.

Experimental

Materials

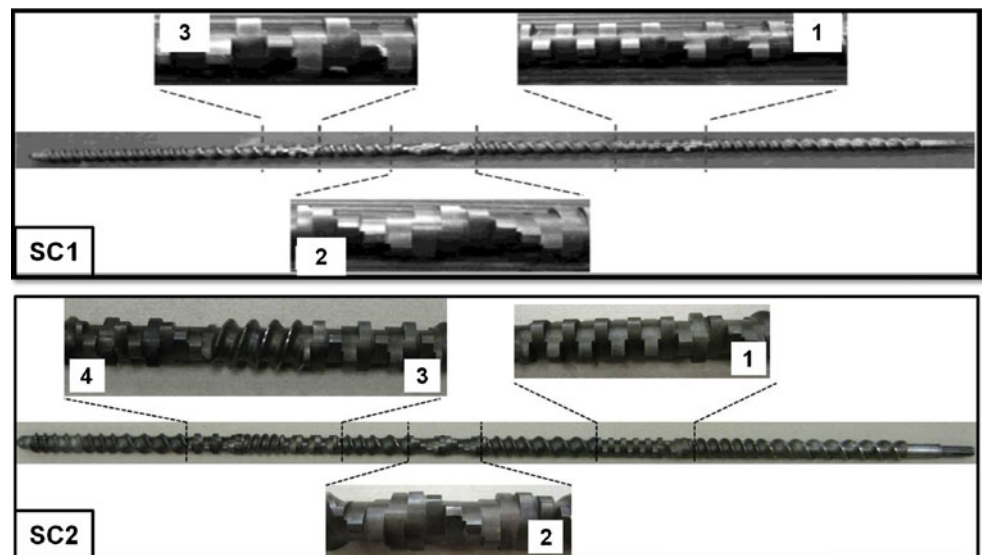
The polyethylene terephthalate used in this study, PET 9921, is a commercial product of Eastman Chemical Company with intrinsic viscosity of 0.8 dL/g and a melting point of 243 °C. The following natural organoclays have been used: C30B, C15A, and Cloisite® 25A (C25A) from Southern Clay Products Inc., and N28E from Nanocor Inc. Unmodified synthetic clay Somasif® ME100 (SM100) from CBC Co. Ltd was also utilized. The chemical composition of the organic modifiers (when applicable), the

interlayer spacing of the clays, and the solubility parameter of the organic modifiers are summarized in Table 1. The content of organic modifier presents in the various organoclays was determined by thermogravimetric analysis (TGA Q500, TA Instruments). For these tests, samples of 10 mg were heated from room temperature to 800 °C with a heating rate of 10 °C/min under an air atmosphere. In Table 1 it is observed that the organoclays *d*-spacing is correlated with the organic modifier content.

Melt compounding

The PET and clay particles were vacuum dried at 90 °C for 24 h before extrusion. A corotating twin-screw Leistritz extruder (screw diameter = 18 mm and $L/D = 40$) was used to prepare samples containing 0–8 wt% of clay particles. Figure 1 depicts two different screw configurations (screw configuration #1 (SC1) and screw configuration #2

Fig. 1 Screw configurations SC1 and SC2



(SC2)) which were used in this study. Both screw geometries have the same conveying and pressuring elements, followed by the first mixing zone with 30°, 60°, and 90° elliptical kneading elements 4 mm thick. The second and third mixing zones, with 30° and 60° elliptical elements, respectively, are also the same for both screw configurations. The only difference is that SC2 has a fourth mixing zone with 30° and 60° elliptical elements and a reverse element located between the third and the fourth mixing zones. It was observed that residence time at 200 rpm increases from 51 s for SC1 to 90 s for SC2. The residence times were estimated, 15 min after starting the extrusion, by adding a colored resin while feeding the neat PET. The measured torque value of the second screw was about 8 % larger than the first one for nanocomposites containing 8 wt% C30B.

The extrusion conditions were the same for both screw configurations. Melt blending was performed at a screw speed of 200 rpm and feeding rate of 2 kg/h. The temperature profile from the feed to the die was set between 240 and 265 °C. To cool the extrudate, a bath containing a mixture of water and ice was used. The extruded samples were granulated and vacuum dried at 90 °C for 24 h. Compression molding was subsequently performed to obtain disk-shape samples of approximately 2-mm thick and 25 mm in diameter by employing a Carver® laboratory press (model 3912) at 265 °C for 9 min at a pressure of 20 MPa and under a blanket of nitrogen, followed by quenching in another Carver® laboratory press (model 30–12 H) for 5 min. The disk-shape samples were vacuum-dried at 90 °C for 24 h before being subjected to rheological testing.

Characterization

WAXD was used to obtain the basal distance of the clay layers by employing a Bruker D8 Discover with Cu k_{α} radiation of wavelength $\lambda = 1.5406 \text{ \AA}$. The generator was operated at 40 kV and 40 mA. The spectra were recorded over a 2θ range of 0.8°–10° using a scan rate of 0.6°/min.

SEM observations were done to evaluate the microscale distribution of the clay particles in the PET matrix using a Field Emission Gun SEM, Hitachi S4700, operating at 2 kV. The specimens were prepared using an Ultracut FC microtome (LEICA) with a diamond knife and then coated with platinum. TEM images were obtained using a JEOL JEM-2100 F microscope operating at 200 kV to assess the quality of clay dispersion in the samples. For TEM imaging, the samples were microtomed into ultrathin slices about 50–80-nm thick at a cryogenic temperature (i.e., –100 °C) using the aforementioned microtome system.

Rheological measurements in oscillatory mode were performed using a Bohlin Gemini rheometer, with a parallel

plate flow geometry (25 mm diameter, 1 mm gap). Time and frequency sweeps in small-amplitude oscillatory shear were carried out on the neat PET and PET-based nanocomposite samples at 265 °C under a nitrogen atmosphere to avoid oxidative degradation. The time sweep test of each sample was repeated twice, always with a fresh specimen, at 0.628 rad/s over 900 s. The frequency sweep tests were repeated four times for each sample, always using a fresh specimen and carried out in the linear regime. Two specimens were subjected to frequency sweep from low to high frequency, and two more from high to low. Strain sweeps were applied at a frequency of 6.28 rad/s and strain amplitudes from 0.01 to 1. After adjusting the gap, the samples were held in quiescent state for 3 min before starting the rheological tests. This should allow orientation relaxation if there was any induced by sample loading. We also verified the effect of gap size on the viscoelastic properties of the nanocomposites at the maximum clay loading of C30B (i.e., 8 wt%). We observed that gap size had no significant effect on the results.

Results and discussion

Morphology of nanocomposites prepared using SC1 XRD patterns of PET nanocomposites with various C30B concentrations are shown in Fig. 2. The nanocomposite samples are denoted with a nomenclature “PET/ xy ”, where x and y denote concentration and type of clay particles, respectively. The gallery spacing of C30B powder (d_{001} diffraction), which is 1.85 nm, increases up to 3.4 nm ($2\theta \approx 2.5^\circ$)

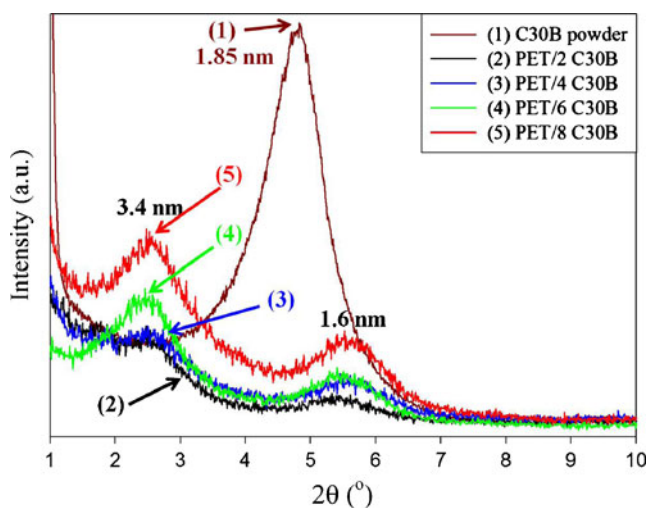


Fig. 2 X-ray diffractograms of PET nanocomposites containing different weight fractions of C30B prepared by screw configuration #1

after being melt blended with PET. The enhancement of C30B basal spacing is due to the diffusion of the PET chains into the interlayer spacing of the layered silicate. Although the peak position of the XRD curves does not change with clay concentration, the intensity of the peaks increases monotonically with clay concentration, which is a sign of more extensive domains of periodicity, (Delozier et al. 2003; Bhattacharya et al. 2007). Note that the second peaks observed at $2\theta \approx 5.2^\circ$ may be attributed to the d_{002} diffraction and/or clay gallery collapse.

Figure 3 shows the SEM micrographs of PET nanocomposites containing 2, 4, 6, and 8 wt% of C30B prepared using SC1. This figure illustrates the state of the clay particles distribution within the PET matrix and the efficiency of SC1 in breaking down C30B aggregates. SEM results also show large aggregates for the nanocomposites at high clay loadings (Fig. 3b–d). It is obvious from the SEM micrographs that the number of kneading elements and the residence time in SC1 for compounding are not sufficient to break down all the large aggregates.

Morphology of nanocomposites prepared using SC2

As the SC1 was not efficient for the compounding, additional kneading elements were employed in screw configuration #2 to increase the shear stresses. In addition, by placing reverse conveying elements between the two last kneading blocks, a longer residence time was achieved for screw configuration #2 in comparison to screw configuration #1 (90 vs. 51 s). Figure 4 presents the SEM micrographs of PET nanocomposites containing 2 and 6 wt% C30B prepared using screw configuration #2. The PET nanocomposite containing 2 wt% C30B exhibits a homogeneous distribution of the clay particles all over the sample (Fig. 4a). Using this screw configuration, even by incorporating 6 wt% C30B, no large aggregates are observed, and the clay particles are well distributed within the PET matrix (Fig. 4b). By comparing the morphologies of PET/6 C30B nanocomposites prepared using screw configurations #1 and #2 (Figs. 3c and 4b, respectively), it is seen that SC2 is more efficient than SC1 in breaking down the large

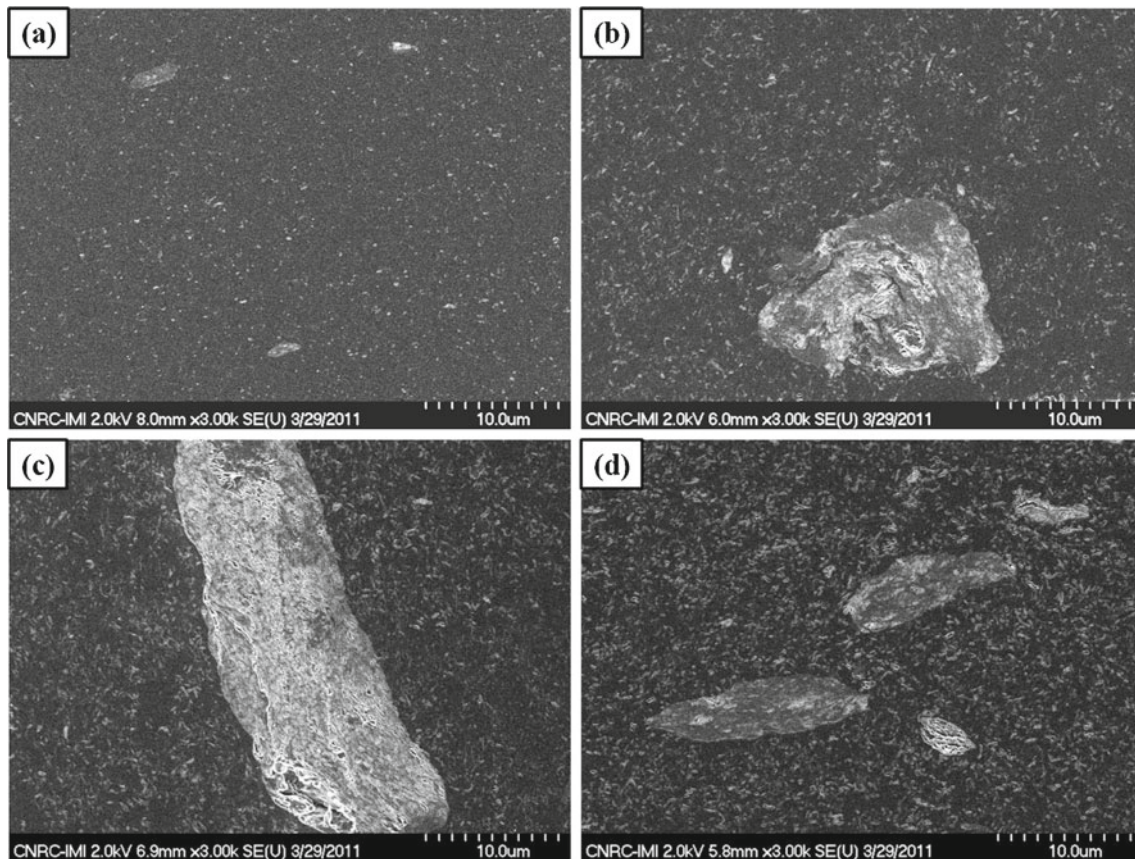


Fig. 3 SEM micrographs of **a** PET/2 C30B, **b** PET/4 C30B, **c** PET/6 C30B, and **d** PET/8 C30B nanocomposites prepared using screw configuration #1

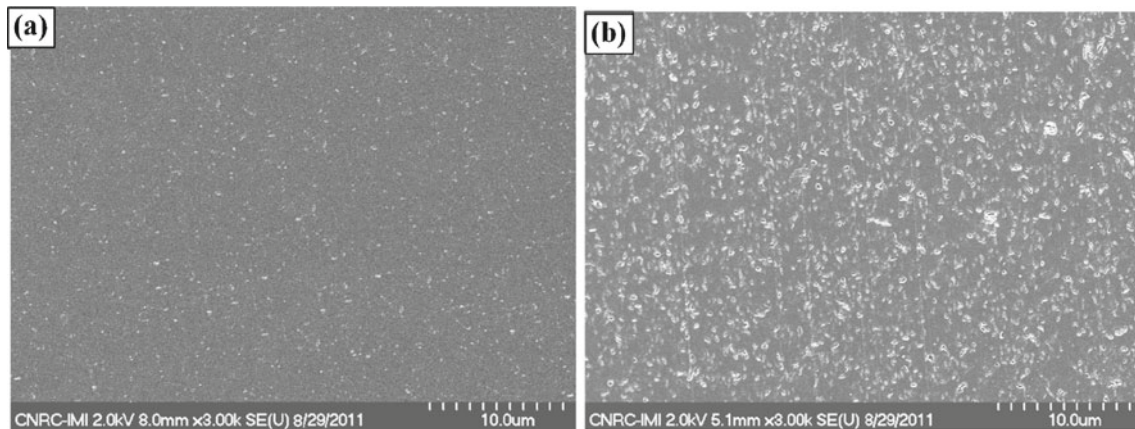


Fig. 4 SEM micrographs of **a** PET/2 C30B and **b** PET/6 C30B nanocomposites prepared using screw configuration # 2

clay aggregates, as expected. Changing the screw configuration did not have a pronounced effect on XRD patterns of nanocomposites in terms of the peak position and shape of the peak (data are not shown here). Based on the poor morphology obtained using SC1, this screw configuration is not discussed further, and all following results were obtained with SC2.

Effect of clay concentration on the rheological properties of PET nanocomposites

Oscillatory time sweep tests were performed to examine if the neat PET and its corresponding nanocomposites had time-dependent rheological properties due to thermal degradation and/or possible chemical reactions between PET and the clay organo-modifiers. The complex viscosity and storage modulus of the neat PET and PET nanocomposites containing 2–8 wt% C30B are shown as functions of time in Fig. 5a, b, respectively (note that by complex viscosity, we mean the modulus of the complex viscosity in the whole text). As stated before, the time sweeps were repeated twice for each sample, always with a fresh specimen, and the results are shown in Fig. 5 in the form of filled and unfilled symbols. These tests confirmed that for all samples, a period of up to 10 min resulted in less than 10 % changes in the viscoelastic properties. The complex viscosity of the PET nanocomposite containing 2 wt% C30B is observed to be lower than that of the neat PET. This is attributed to the severe degradation of the PET matrix in the presence of the organoclay. This aspect is discussed in more details below. A lower complex viscosity for PET nanocomposites containing 2 wt% of N28E and C30B in comparison to the same neat PET has been reported before (Ghanbari et al. 2012; Xu et al. 2011). For the nanocomposites containing 4, 6, and 8 wt%, the linear viscoelastic properties increase markedly with clay loading. For example, the PET/8 C30B sample is more than 20 times more viscous than the neat PET.

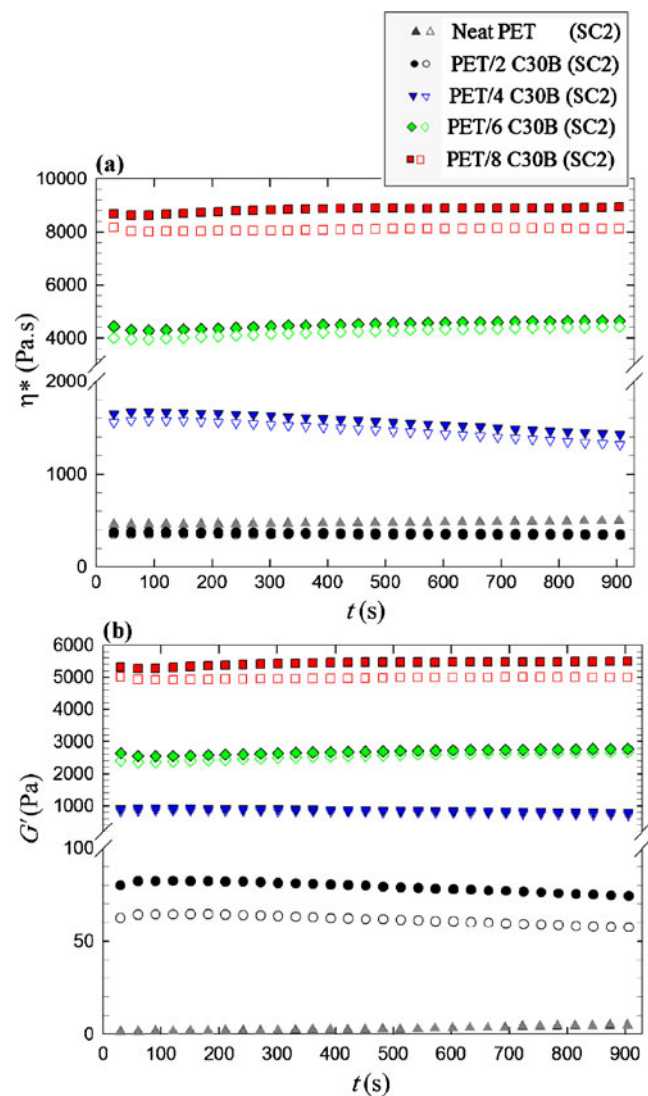


Fig. 5 Complex viscosity **(a)** and storage modulus **(b)** as functions of time for the neat PET and PET/C30B nanocomposites

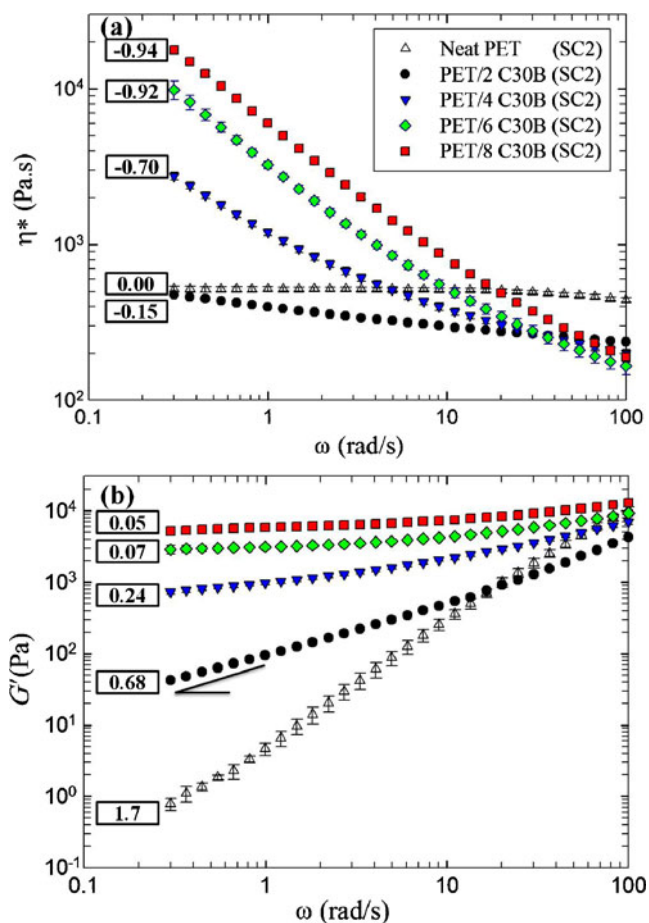


Fig. 6 Complex viscosity (a) and storage modulus (b) of PET/C30B nanocomposites (frequency sweep tests). Numbers in the text boxes represent the η^* and G' slopes at low frequencies

The complex viscosity and storage modulus as functions of frequency for the neat PET and PET-based nanocomposites with various C30B loadings are presented in Fig. 6a, b, respectively. While the neat PET displays a pseudo-Newtonian behavior, the nanocomposites exhibit a marked solid-like behavior (Fig. 6a), which becomes stronger with C30B concentration. Except for the sample containing 2 wt% C30B, the complex viscosity of PET increases with clay concentration at low frequencies. It seems that the incorporation of a small amount of C30B (2 wt%) lowers considerably the complex viscosity of the PET matrix. This behavior has been reported previously (Ghanbari et al. 2012; Wang et al. 2011). At low clay concentration, particle–particle interactions are not pronounced, and the viscosity of PET nanocomposites is governed by the host polymer matrix. It has been well documented that the presence of organoclays leads to a severe chain scission of a PET matrix (Davis et al. 2002; Todorov and Viana 2007; Stoeffler et al. 2008; Litchfield et al. 2010). At high frequencies, where the behavior of the matrix is dominant, all PET nanocompos-

ites show a smaller viscosity than that of the neat polymer, which again can be attributed to the degradation induced by the presence of the organoclay.

One approach to determine the apparent viscosity of the degraded matrix in the nanocomposites is to use the Maron–Pierce empirical model:

$$\frac{\eta^*}{\eta_M^*} = \left(1 - \frac{\varphi}{\varphi_m}\right)^{-2} \tag{1}$$

where η^* and η_M^* are the complex viscosity of the nanocomposite and the matrix, respectively, φ is the volume fraction of the clay, and φ_m is the maximum packing volume fraction which is set here as $\varphi_m = \frac{3.55}{p}$, where p is the clay aspect ratio (Sun et al. 2009; Wan et al. 2012). The aspect ratio of the clay particles was determined by the method described by Ghasemi et al. (2012). In that method, TEM images are used to determine the length-to-thickness ratio of clay particles. For overlapped tactoids, the average thickness and overall length were used, while an end-to-end vector was considered for length of curved tactoids. A value of 46 was obtained for the average aspect ratio of the silicate particles in the PET matrix. Ghasemi et al. (2012) and Fornes and Paul (2003) reported values of 47 and 57, respectively, for the aspect ratio of C30B layered silicates in nanocomposites prepared by melt blending.

The matrix apparent viscosity, $\eta_{M(100 \text{ rad/s})}^*$, is evaluated at 100 rad/s where the contribution of the matrix should be dominant, using the Maron–Pierce empirical model (Eq. 1). The calculated apparent matrix viscosity is presented in Table 2 for the neat PET and PET-based nanocomposites. From the apparent matrix viscosity, it is possible to estimate an apparent matrix molecular weight in order to quantify the degradation induced by the presence of the organoclay. To this end, the classical relationship between the zero-shear

Table 2 Apparent complex (\approx zero-shear) viscosity and apparent molecular weight for the neat PET and the PET matrix in nanocomposites calculated from Eqs. 1 and 2, respectively

Sample	Matrix apparent complex viscosity at 100 rad/s	Matrix apparent molecular weight (kg/mol)
Neat PET	440	65.0*
PET/2 C30B	174	49.5
PET/4 C30B	98	41.8
PET/6 C30B	51.9	34.7
PET/8 C30B	30.9	29.8
PET/6 C15A	57	35.6
PET/6 N28E	64.6	37.0
PET/6 C25A	91.6	41.0

*This value is reported based on the works of Fox et al. (1997) and Champagne et al. (1999) using the same grade of PET

viscosity, η_0 , and the weight average molecular weight, M_w , has been used, assuming a pseudo-Newtonian behavior for the PET matrix:

$$\eta_{M(100 \text{ rad/s})}^* \approx \eta_0 = kM_w^{3.4} \quad (2)$$

where k is taken as 3.02×10^{-4} (Pa.s.mol^{3.4}/kg^{3.4}) by considering the neat PET molecular weight and complex viscosity. The apparent matrix molecular weight is reported in Table 2 for the neat PET and PET-based nanocomposites. Both the zero-shear viscosity and molecular weight of the PET matrix for PET/C30B nanocomposites are found to strongly decrease with clay concentration, and this behavior is attributed to the severe degradation (i.e., chain scission) of the PET matrix in the presence of the organoclay. It explains the lower complex viscosity for the nanocomposites at high frequencies observed in Fig. 6a, in comparison to the neat sample. The results for the apparent matrix viscosity and apparent matrix molecular weight of PET nanocomposites containing 6 wt% C15A, C25A, and N28E reported in Table 2 will be discussed later.

The effect of C30B content on the storage modulus of the PET nanocomposites can be observed in Fig. 6b. The storage modulus increased significantly with C30B concentration at low frequencies. With increasing clay loading, the dependence of storage modulus on frequency decreases (slope of G' vs. ω at low frequencies reported in text boxes), and at high clay concentrations (6 and 8 wt%), the storage modulus is nearly independent of frequency at low frequencies. This pseudo-solid-like behavior is attributed to the formation of a space-filling interconnected network of clay particles. This percolated three-dimensional network acts like a weak solid and causes significant enhancement of the storage modulus, as well as the emergence of a low-frequency plateau (Mobuchon et al. 2007; Aubry et al. 2005; Eslami et al. 2010; Solomon et al. 2001; Vermant et al. 2007; Wu et al. 2005; Mobuchon et al. 2009a; Pujari et al. 2011). Although the incorporation of 2 wt% C30B in the PET matrix enhances the low frequency storage modulus, a sharp increment is seen when the clay concentration reaches 4 wt%, implying the formation of a percolated network.

Figure 7 shows the reduced viscosity and reduced storage modulus of the neat PET and PET nanocomposites containing 2–8 wt% C30B as functions of angular frequency. The reduced viscosity (Fig. 7a) is obtained by taking the ratio of the magnitude of the complex viscosity of the various samples to the matrix apparent viscosity estimated at 100 rad/s (Table 2). It is observed that the reduced viscosity increases with clay content on the whole frequency range. Hence, the normalization allows removing thermal degradation effects to highlight the clay contribution. The reduced viscosity of the PET nanocomposites exhibits a very strong solid-like behavior at high clay loadings with a slope on the

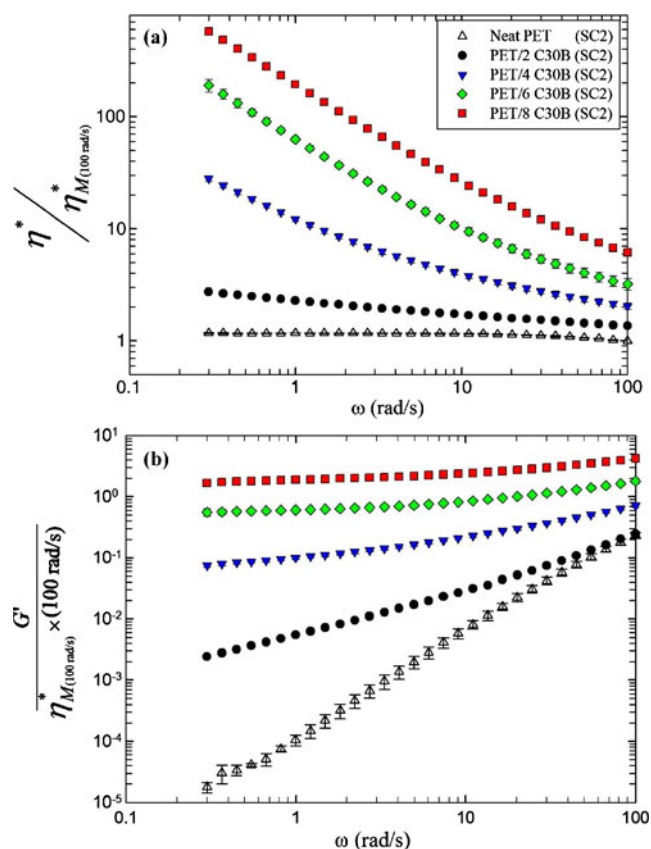
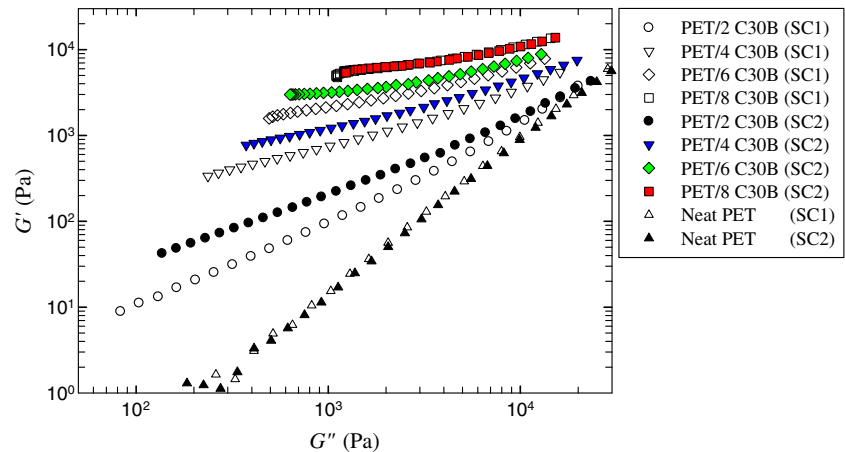


Fig. 7 Reduced viscosity (a) and reduced storage modulus (b) of the neat PET and PET/C30B nanocomposites as functions of clay loading and frequency.

log–log plots approaching -1 . The reduced storage modulus (Fig. 7b) is obtained by taking the ratio of the magnitude of the storage modulus of the various samples to the matrix apparent viscosity estimated at 100 rad/s (Table 2) and the frequency equal to 100 rad/s. It also increases with clay concentration and exhibits a low frequency plateau at high clay loadings. It is noteworthy to mention that the reduced storage modulus of the neat PET does not exceed the reduced storage modulus of PET nanocomposites at high frequencies, as previously seen in Fig. 6a when thermal degradation effects are not accounted for.

Figure 8 reports plots of the elastic modulus vs. the loss modulus for the neat PET and the PET nanocomposites containing 2–8 wt% C30B and prepared using screw configurations #1 and #2. First, we note that the screw geometry had little effect on the neat PET and that data of the neat PET processed with screw configuration #2 are slightly shifted down, suggesting possibly more degradation of the PET with that geometry. However, the differences are within the experimental error. PET nanocomposites containing 2, 4, and 6 wt% C30B and prepared using screw configuration #2 exhibit larger values of the elastic modulus in compari-

Fig. 8 Storage modulus vs. loss modulus for the neat PET and the PET/C30B nanocomposites prepared using screw configurations #1 (SC1) and #2 (SC2)



son to those prepared using screw configuration #1. These observations suggest that a better dispersion of C30B particles is obtained by employing screw configuration #2, in good agreement with SEM micrographs of Figs. 3 and 4. The data for the PET/8 C30B nanocomposites prepared by screw configurations #1 and #2 are, however, very similar. It seems that when the clay concentration is very high, even the more severe screw geometry cannot help breaking down the large aggregates and disperse further the nanoparticles. Consequently, morphologies similar to that presented in Fig. 3d are expected for PET/8C30B nanocomposites prepared using screw configuration #2. This may be attributed to the lack of sufficient space for the dispersion of clay particles, as the C30B volume fraction is equal to 0.046, which is close to the maximum packing volume fraction ($\varphi_m = 3.55/p = 0.077$). Hence, some clay tactoids may remain undelaminated. Therefore, we may expect a lower level of exfoliation and higher number of clay aggregates at increasing clay concentration, which will be proven later in this study using image analysis. At high clay loadings, plots of G' vs. G'' (Fig. 8) exhibit a pseudo-solid-like behavior for both screw configurations, indicating the presence of an interconnected network of individual clay platelets and/or intercalated tactoids acting like a weak solid. The differences between the elastic modulus of PET nanocomposites prepared using screw configurations #1 and #2 are more pronounced at low values of the loss modulus (low frequencies) where the effect of clay particles is more pronounced.

As observed earlier in Fig. 7b, a significant increase (almost four orders of magnitude with respect to the neat PET) of the low frequency G' of PET nanocomposites takes place for the clay concentration of 4 wt%, and the rheological behavior changes from liquid- to solid-like. These observations suggest that percolation must happen when the C30B concentration increases from 2 to 4 wt%.

The value of the elastic modulus at low frequencies ($\omega = 0.3$ rad/s) was used to determine the percolation threshold

for PET/C30B nanocomposites. The following percolation model (Vermant et al. 2007; Khalkhal et al. 2011) was used:

$$G' \propto (\varphi - \varphi_{per})^n \tag{3}$$

where φ_{per} and n are the percolation threshold volume fraction and a power-law exponent, respectively. The parameter n is equal to 1.68 and 1.07 for screw configurations #1 and #2, respectively. The calculated percolation values (in wt%) are 3.4 and 3.2 for PET/C30B nanocomposites prepared using screw configuration 1 and 2, respectively, hence between 2 and 4 wt% as suggested by Figs. 6b and 7b. It seems that the screw configuration and residence time does not impact much the value of the percolation threshold, which is somehow surprising.

The pseudo-solid-like behavior of the storage modulus at low frequencies indicates the existence of a yield stress for these systems. To observe this effect more clearly, we plot the complex viscosity vs. complex modulus in Fig. 9 as a function of C30B concentration. A sharp increase of the complex viscosity as the complex modulus decreases

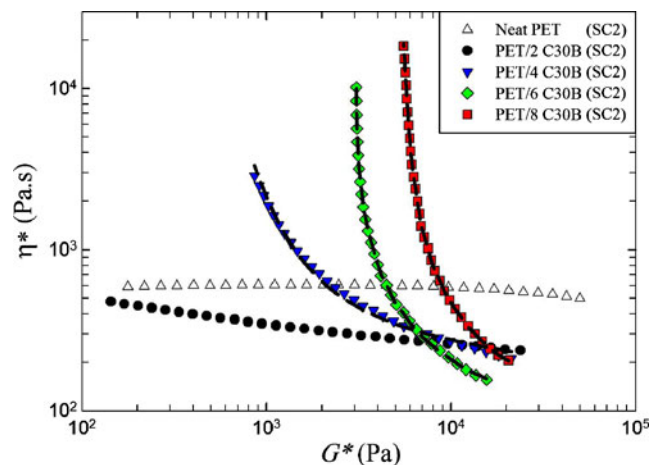


Fig. 9 Complex viscosity vs. complex modulus for neat PET and PET/C30B nanocomposites. Dashed lines are fits of Eq. 4 for clay content above 2 wt%

Table 3 Herschel–Bulkley parameters for the PET nanocomposites

Sample	$\sigma_0 = G_0^* \times \gamma^0$ (Pa)	k (Pa.s ^{<i>n</i>})	n
PET/4 C30B (SC2)	25.7	257	0.88
PET/6 C30B (SC2)	91.8	152	0.85
PET/8 C30B (SC2)	166	189	0.78
PET/6 C25A (SC2)	69.5	417	0.82
PET/6 C15A (SC2)	43.4	215	0.84
PET/6 N28E (SC2)	41.8	266	0.82

indicates the existence of an apparent yield stress. This representation highlights clearly the presence of a yield stress in the PET nanocomposites with clay concentration above the percolation threshold of ~ 3 wt%. The presence of an apparent yield stress was also observed by other researchers for various nanocomposite systems (Mitchell and Krishnamoorti 2002; Abbasi et al. 2009; Mobuchon et al. 2007; Galgali et al. 2001; Aubry et al. 2005).

To estimate the apparent yield stress, a modified Herschel–Bulkley model is used as follows:

$$\eta^* = \frac{G_0^*}{\omega} + k (\gamma^0 \omega)^{n-1}, \quad (4)$$

where G_0^* is the magnitude of the complex modulus (called complex modulus for simplicity) at the lowest frequency, γ^0 is the strain amplitude, k is a constant, and n is the flow index which determine the behavior of the fluid.

It has been observed that yield stress, $\sigma_0 = G_0^* \gamma^0$, and n can be related to the microstructure of nanocomposites (Xia and Song 2006; Litchfield and Baird 2006). A lower value of n means a higher shear-thinning behavior, which corresponds to a stronger network. Therefore, it is reasonable to expect a lower value of n when clay concentration increases. Besides, stronger particle–particle and/or polymer–particle interactions results in larger apparent yield stresses (Litchfield and Baird 2006). Table 3 lists the calculated Herschel–Bulkley parameters for the PET-based nanocomposites, and the fits of Eq. 4 are shown by the dashed lines in Fig. 9 for the PET/C30B nanocomposites. The Herschel–Bulkley parameters for PET nanocomposites containing 6 wt% C15A, C25A, and N28E will be discussed later. PET nanocomposites containing C30B exhibit larger values of the yield stress at the same clay concentration. This is indicative of the stronger affinity of C30B for PET compared to the other clays. The parameter n decreases slightly with clay content, implying the formation of a stronger network at high clay loadings.

It has been reported that the limit of linearity, γ_c^0 , of filled systems is very sensitive to filler content (Yziquel et al. 1999; Eslami et al. 2010; Aubry et al. 2005; Khalkhal and Carreau 2011; Vermant et al. 2007). Figure 10 shows the normalized storage modulus (i.e., G'/G'_0 , where G'_0 is

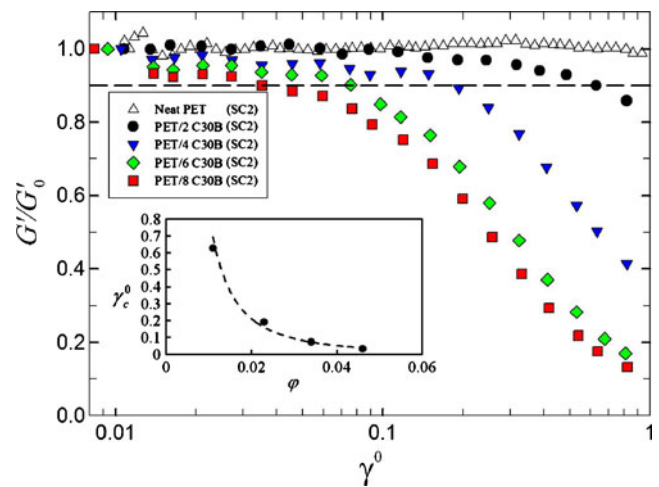


Fig. 10 Normalized storage modulus vs. strain amplitude for the neat PET and PET/C30B nanocomposites at 6.28 rad/s. The inset shows the maximum strain amplitude for the linear viscoelastic behavior as a function of the clay volume fraction

the storage modulus at the smallest strain) as a function of strain, γ^0 , for the neat PET and PET/C30B nanocomposites at 6.28 rad/s. The dashed line indicates the transition from the linear to nonlinear behavior, which is defined as the threshold where the storage modulus decreases by more than 10 % from its value at the smallest strain (i.e., $G'/G'_0 < 0.9$) (Khalkhal and Carreau 2011). Nonlinearity appears at lower strain as the C30B concentration increases. Clay particles are solid, so the straining motion is totally concentrated in the polymer melt, which increases the effective deformation of the matrix and reduces the linearity limit (Vermant et al. 2007). The inset in Fig. 10 illustrates the maximum strain amplitude for the linear viscoelastic behavior as a function of the clay volume fraction. It is observed that critical strain displays a power-law dependency on the volume fraction of C30B, which is approximated by the following relation:

$$\gamma_c^0 \propto \phi^{-2}. \quad (5)$$

The effect of clay chemistry on the morphology and rheology of PET nanocomposites

The morphology of a polymer nanocomposite, which governs the final properties, is not only dependent on particle–particle interactions but also on the degree of compatibility between the polymer matrix and the organoclay that rules polymer–particle interactions. Therefore, the existence of strong interactions between silicate layers and a host polymer matrix is essential to achieve desirable properties. In this work, in addition to various organo-modified clays (C30B, C15A, C25A, and N28E), the effect of a pristine

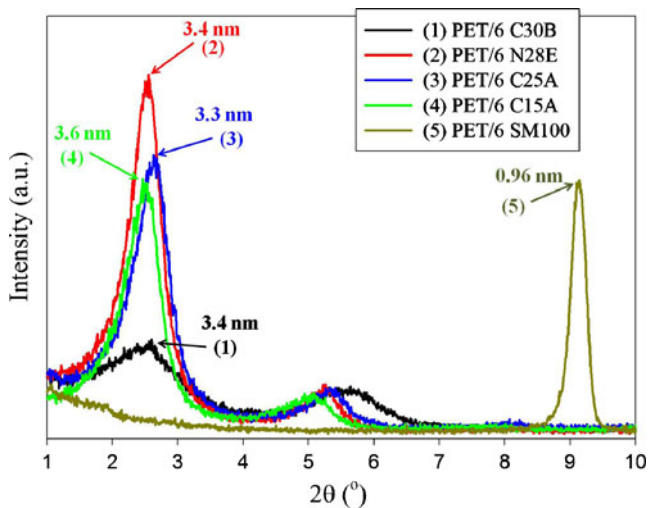


Fig. 11 XRD patterns of PET nanocomposites containing 6 wt% clay particles prepared using screw configuration #2

synthetic clay (i.e., SM100) is examined. PET nanocomposites containing 6 wt% of different clays were prepared using screw configuration #2, and their corresponding XRD patterns are shown in Fig. 11. As expected, the PET chains are not able to diffuse within the gallery spacing of SM100 layered silicate, and the gallery spacing remains the same as the clay alone (Table 1). The largest increases of the basal spacing, 1.55 and 1.44 nm, were obtained for C30B and C25A, respectively. The gallery spacing of N28E and C15A shows only 1.0 and 0.45 nm enhancement in their corresponding PET nanocomposites. Therefore, higher viscoelastic properties are expected for PET nanocomposites containing C30B and C25A, in comparison to those containing N28E or C15A. It has been also shown by other researchers that the higher surfactant content of C15A, which results in a high initial gallery spacing, does not guarantee a higher intercalation in a polymer matrix (Hyun et al. 2001; Ray and Bousmina 2005).

Figure 12 reports the complex viscosity and storage modulus of the neat PET and PET nanocomposites containing 6 wt% of C30B, C15A, C25A, and N28E prepared using screw configuration #2. All PET nanocomposites exhibit a solid-like behavior. These rheological observations are in good agreement with the XRD results: the lower peaks shown in Fig. 11 at $2\theta = 2.5^\circ$ suggest a better clay dispersion for C30B and C25A in comparison to N28E and C15A, resulting in larger values for the complex viscosity and storage modulus at low frequencies.

The solubility parameter, δ , of the different organoclay surfactants was calculated based on the Fedors group contribution method to evaluate the extent of compatibility of PET with the various organoclays (Van Krevelen and te Nijenhuis 2009). According to the solubility parameters presented in Table 1, the order of favorable interactions between

PET and the organoclays is: C30B>C25A>C15A>N28E, which is in good agreement with the rheological observations.

As mentioned earlier, the yield stress can be used to quantify the solid-like character of nanocomposites. Larger yield stress means better dispersion of clay particles in nanocomposites at the same clay concentrations (Litchfield and Baird 2006; Xia and Song 2006). The Herschel–Bulkley parameters for PET nanocomposites containing 6 wt% of different organoclays are reported in Table 3. Experimental data of the complex viscosity vs. complex modulus are shown in Fig. 13, along with the fits of Eq. 4 (dashed lines). The values of the apparent yield stress exhibit the following order for PET nanocomposites containing the different organoclays: C30B>C25A>C15A>N28E, in good agreement with the order of favorable interactions between PET and the organoclays based on the solubility parameter. It is observed, however, that the parameter n of the PET nanocomposites containing the various organoclays

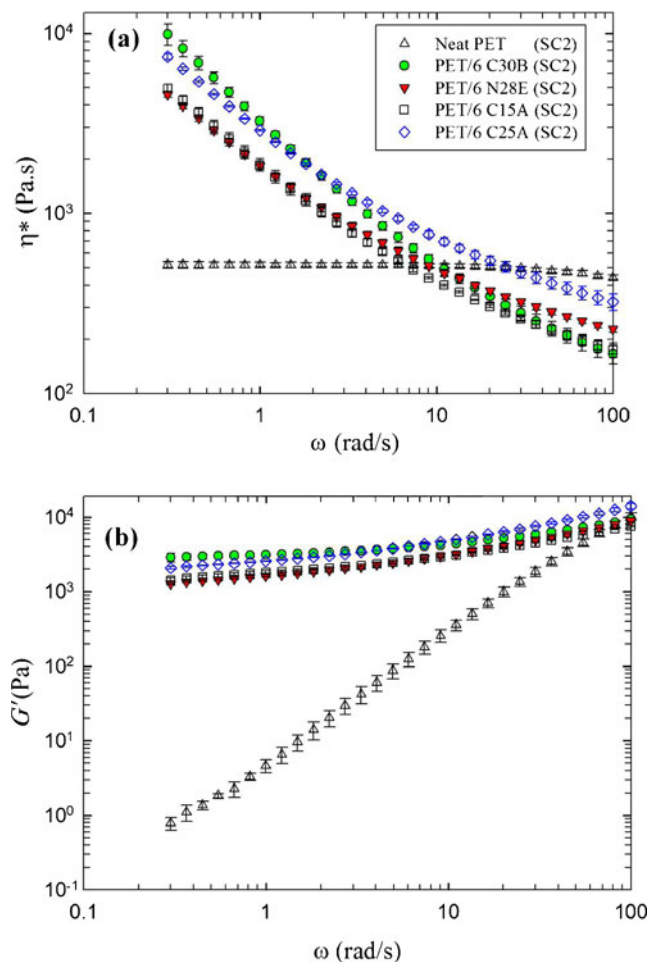


Fig. 12 Complex viscosity (a) and storage modulus (b) for PET nanocomposites containing 6 wt% organoclays prepared using screw configuration #2 (SC2)

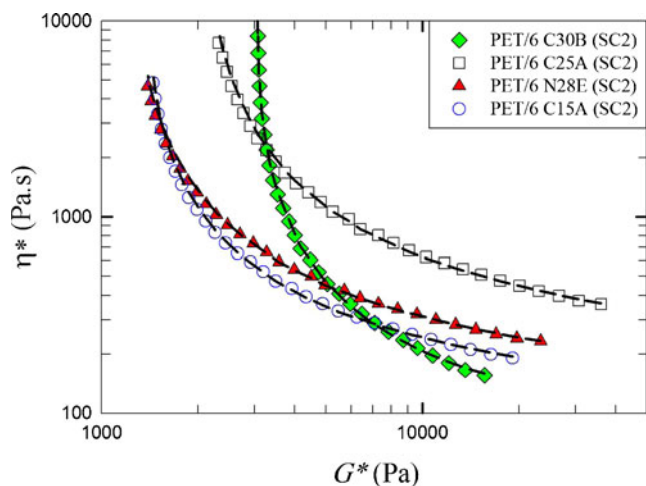


Fig. 13 Complex viscosity vs. complex modulus for PET nanocomposites containing 6 wt% of various organoclays. Dashed lines are fits of Eq. 4

is almost the same; hence, the behavior of the different suspensions does not change much. The better morphology and rheological properties obtained for nanocomposites containing C30B are attributed to the favorable interactions between carboxyl groups of the PET chains and hydroxyl groups of the C30B organic modifier (Ghasemi et al. 2011b).

As done above, the apparent viscosity and apparent molecular weight of the degraded PET matrix in the nanocomposites containing 6 wt% of different organoclays are reported in Table 2. It is observed that the reduction of the PET matrix apparent molecular weight and apparent viscosity is dependent on the surfactant chemistry of the organoclay (Table 1). The highest degradation occurs for the matrix containing C30B, which can be attributed to the specific organic modifier of this organoclay. Previous studies have shown that a better dispersion of organoclays increase the exposure of silicate nanoplatelet surfaces to the polymer matrix and results in a higher level of thermal degradation (Fornes et al. 2003). In addition, organoclays modified with unsaturated tallow that contain double bonds in their alkyl chain result in a greater degradation in comparison to those modified with hydrogenated tallow (Yoon et al. 2003). Surfactants with double bonds are prone to free radical formation and induce more chain scission, as the free radicals can attack polymer chains. It has also been shown that organic modifiers possessing hydroxyl-ethyl groups lead to more degradation than those having methyl groups (Fornes et al. 2003; Yoon et al. 2003). As C30B has the highest level of exfoliation in the PET matrix and its organic modifier contains unsaturated tallow as well as hydroxyl-ethyl groups (Table 1), a higher level of thermal degradation is expected for PET nanocomposites containing this organoclay. This is confirmed by the lowest apparent molecular weight reported

in Table 2 (34.7 kg/mol) for a 6 wt% clay content. The amount of organic modifier used in the treatment of C15A is larger than the cation exchange capacity of the pristine montmorillonite (125 vs. 92.6 meq/100 g clay, an excess of nearly 35 %). This excess gives rise to unbound surfactant that may cause more degradation (Mittal 2011; Cui et al. 2008). N28E has 25 % excess of the organic modifier, while C25A bear an excess of only 2.6 %. The unbound surfactant of C15A and N28E can result in a significant degradation of the PET matrix, as confirmed by the low apparent molecular weights of 35.6 and 37 kg/mol reported in Table 2 for PET/6 C15A and PET/6N28E, respectively. In contrast, C25A yields the lowest thermal degradation, as confirmed by the largest apparent molecular weight reported in Table 2 (41 kg/mol) for the nanocomposites containing 6 wt% C25A.

Figure 14 presents the reduced complex viscosity and reduced storage modulus vs. frequency for the neat PET and PET nanocomposites containing 6 wt% C30B, C15A, C25A, and N28E prepared using screw configuration #2. The reduced viscosity of all the PET nanocomposites is now larger than that of the neat PET, even at 100 rad/s,

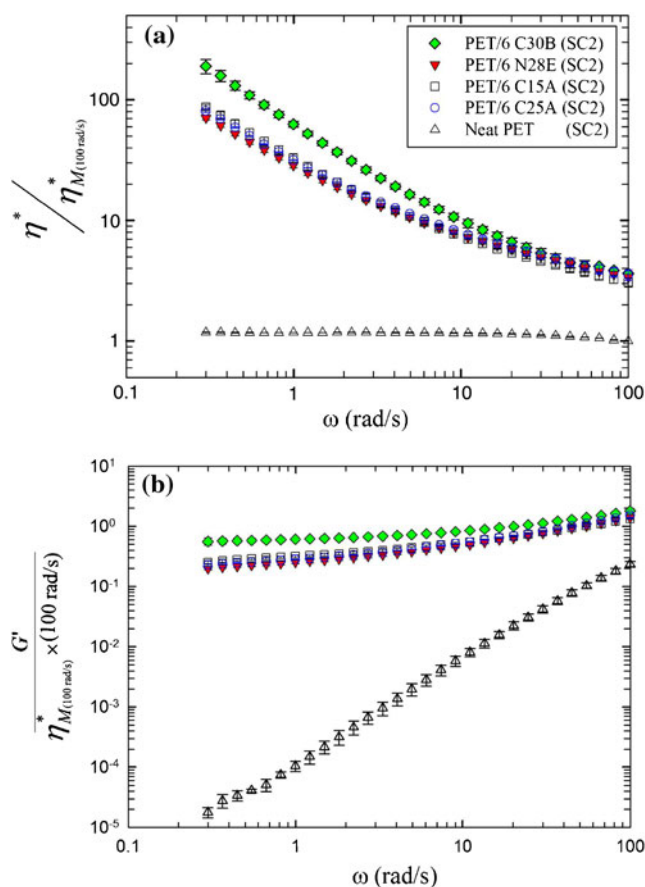


Fig. 14 Reduced viscosity (a) and reduced storage modulus (b) for neat PET and PET nanocomposites containing 6 wt% C30B, C15A, C25A, and N28E prepared using screw configuration #2

and it shows a remarkable solid-like behavior. Hence, again the normalization allows removing the effect of the PET matrix thermal degradation. As expected, PET nanocomposites containing C30B and N28E exhibit the largest and the smallest reduced complex viscosities, respectively. The reduced storage modulus of PET nanocomposites containing 6 wt% of the different organoclays is larger than that of the neat PET on the whole frequency range. The largest and the smallest reduced storage modulus are exhibited by the PET nanocomposites containing C30B and N28E, respectively. It is of interest to look more closely at their respective morphologies in order to correlate with the rheological behavior.

SEM and TEM techniques were used to examine the state of spatial distribution and dispersion of C30B and N28E particles in the PET matrix. Figure 15 presents SEM micrographs of PET nanocomposites containing 6 wt% C30B and N28E prepared using screw configuration #2. There are more empty spaces neighboring N28E particles than C30B particles. It seems that PET nanocomposites containing C30B exhibit higher clay density than those containing N28E. Based on the SEM observations, more particle–particle and polymer–particle interactions are expected for this nanocomposite, due to the higher clay density resulting from fewer aggregates. The interpretation of the SEM micrographs is in good agreement with the XRD (Fig. 11) and rheological results (Fig. 14).

Typical TEM bright field images of PET nanocomposites containing 2 and 6 wt% C30B and those containing 6 wt% N28E are shown in Fig. 16. Both individual platelets and tactoids are seen in the images. It is not easy to differentiate PET nanocomposites containing 2 and 6 wt% C30B based on the high magnification of the TEM images. A better exfoliation of C30B in comparison to N28E in the corresponding PET nanocomposites is obvious at both low and high magnification TEM images. Again, TEM results are in good

agreement with XRD, SEM, and rheology results presented before.

To quantify the degree of layer dispersion in the PET nanocomposites, a technique based on free-path spacing distance introduced by Luo and Koo is used (2007, 2008). In this method, the free-path distance between the platelets is measured by drawing random lines (usually horizontal and/or vertical) to intercept silicate layers in a TEM image. After measuring the free-path distance between the platelets, the dimensionless dispersion value, $D_{0.1}$, is calculated based on the distribution of the free-path spacing distances between the clay layers according to the following equation:

$$D_{0.1} = 1.1539 \times 10^{-2} + 7.5933 \times 10^{-2} (\mu/\sigma) + 6.6838 \times 10^{-4} (\mu/\sigma)^2 - 1.9169 \times 10^{-4} (\mu/\sigma)^3 + 3.9201 \times 10^{-6} (\mu/\sigma)^4 \quad (6)$$

where μ is the mean spacing between the clay layers, and σ is the standard deviation.

A value below 4 % for $D_{0.1}$ suggests an immiscible system or microcomposite, and values over 8 % indicate an exfoliated structure, while values between 4 and 8 % indicate intercalation. For approximately 400 measurements for each sample, performed on several TEM images, $D_{0.1}$ values of 5.8, 5.5, and 4.3 % were obtained for PET/2 C30B, PET/6 C30B, and PET/6 N28E nanocomposites, respectively. We obtained a $D_{0.1}$ value of 7.5 for a PET/2 wt% C30B, but in drawn films prepared via a larger twin-screw extruder (Ghanbari et al. 2012). The larger dispersion value for PET/6 C30B in comparison to that of PET/6 N28E indicates a higher level of intercalation, in agreement with the XRD patterns and SEM micrographs. On the other hand, a reduction of the $D_{0.1}$ value with clay concentration indicates that the level of clay exfoliation is less when the clay loading increases.

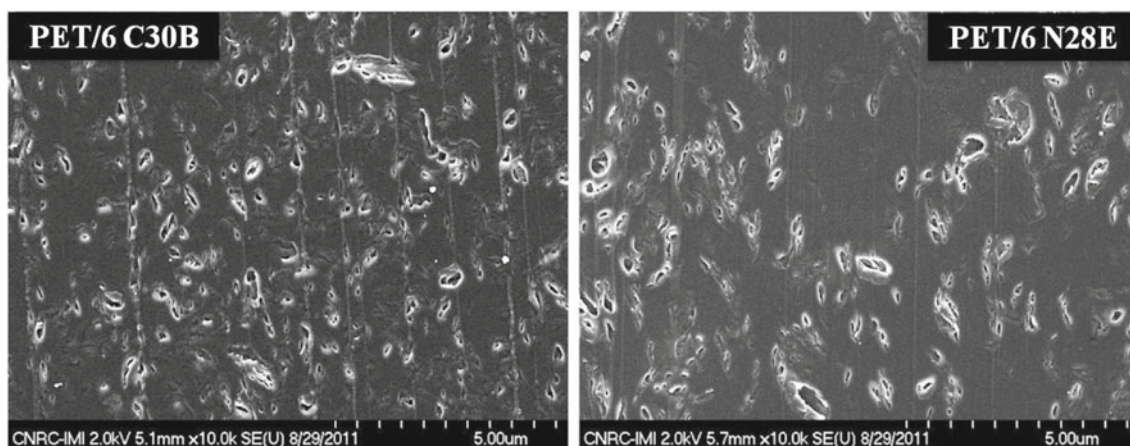


Fig. 15 SEM micrographs of PET nanocomposites containing 6 wt% C30B and N28E prepared using screw configuration #2

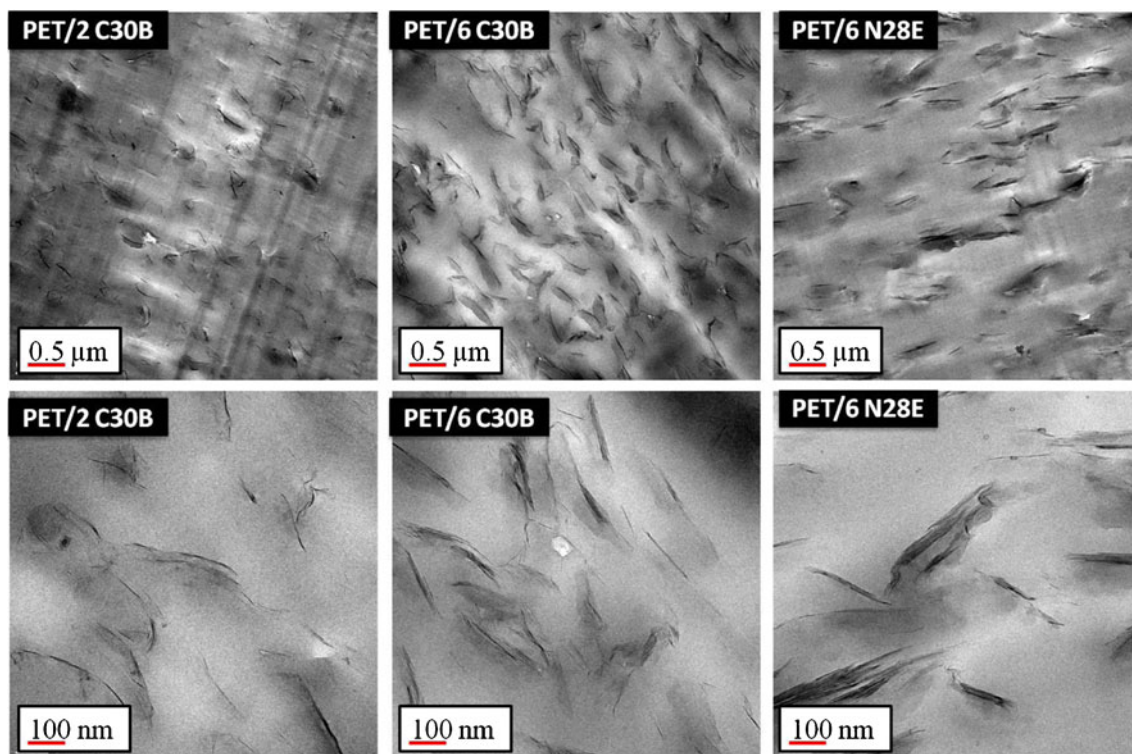


Fig. 16 TEM images of PET/2 C30B, PET/6 C30B, and PET/6 N28E nanocomposites prepared by screw configuration #2 at low and high magnifications

To quantify the effect of clay chemistry and concentration on the morphology of PET nanocomposites, the number of layers per clay particle was manually counted using the TEM images. Figure 17 shows the number of platelets per clay particle histograms for PET nanocomposites containing 2 and 6 wt% C30B and that for the nanocomposite containing 6 wt% N28E. Around 400 particles were counted to ensure statistical validity of the analysis. As expected, the count for clay aggregates increases at higher clay loadings by comparing the PET/2 C30B and PET/6 C30B nanocomposites. The count for single layers and double layer particles is also larger for PET/6 C30B in comparison to PET/6 N28E. On the other hand, the frequency of clay aggregates (five or more layers) is higher for the nanocomposite containing N28E. Favorable interactions between layered silicates and the polymer matrix enhance diffusion of polymeric macromolecules into the gallery spacing of the clay platelets and result in morphologies with higher level of exfoliation. Among the organoclays studied in this work, C30B is the only one that has hydroxyl groups. The highest level of PET chains intercalation into the gallery spacing of C30B in comparison to other organoclays, based on XRD results, is attributed to the favorable interactions between the carboxyl groups of the PET backbone and the hydroxyl groups present in the organo-modifier of C30B. Hence, the higher initial gallery spacing of N28E in comparison to that

of C30B (Table 1) does not help further intercalation of PET macromolecules. Besides, the solubility parameter of PET is closer to that of C30B in comparison to N28E, implying that C30B is more miscible with PET.

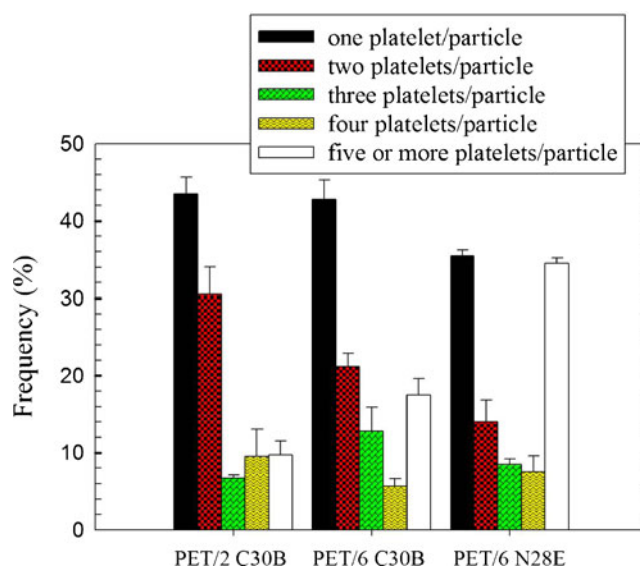


Fig. 17 Number of platelets per particle histogram. The total number of counted particles for each sample was around 400

Conclusion

In this work, PET nanocomposites containing C30B, C15A, C25A, N28E, and SM100 were prepared by melt compounding using a twin-screw extruder. The effect of the screw geometry, clay concentration, and surfactant chemistry of the organoclays on the morphology and rheology of the PET nanocomposites were investigated using XRD, SEM, TEM, and rheometry. The relationship between the microstructure and rheological behavior of the nanocomposites was discussed. It is observed that increasing residence time and employing more shearing elements help breaking and dispersing clay tactoids and improve the viscoelastic properties. Although gallery spacing was found to be independent of the silicate concentration, the count for exfoliated layers was higher for nanocomposites based on C30B and decreased with clay concentration. The complex viscosity of PET nanocomposites exhibits a solid-like behavior, which becomes stronger with clay loading. The storage modulus shows a pseudo-solid-like behavior at low frequencies and high clay concentrations, due to the formation of a percolated network. The apparent yield stress in nanocomposites has been determined using the Herschel–Bulkley model, and it was shown to increase with clay concentration and level of exfoliation. Among the various organoclays studied in this work, those being more intercalated with the PET chains exhibited larger rheological properties. The largest values of the complex viscosity and storage modulus as well as the highest degree of intercalation were obtained for C30B, which has the solubility parameter value closer to that of PET. The degradation of PET chains in the nanocomposites due to the presence of organoclays led to a lower complex viscosity for PET nanocomposites in comparison to the neat sample at high frequencies. It was possible to account for the degradation of the PET matrix by using the Maron–Pierce equation for the high-frequency data. The molecular weight of the PET matrix was found to decrease from 65 kg/mol for the neat PET to 29.8 kg/mol for the PET nanocomposite containing 8 wt% C30B.

Acknowledgements The authors are thankful to Mrs. W. Leelapornpisit for the SEM and TEM analysis. Financial support from NSERC (Natural Science and Engineering Research Council of Canada) in the context of the NRC-NSERC-BDC Nanotechnology Initiative is gratefully acknowledged.

References

- Abbasi S, Carreau PJ, Derdouri A, Moan M (2009) Rheological properties and percolation in suspensions of multiwalled carbon nanotubes in polycarbonate. *Rheol Acta* 48(9):943–959. doi:10.1007/s00397-009-0375-7
- Aubry T, Razafinimaro T, Mederic P (2005) Rheological investigation of the melt state elastic and yield properties of a polyamide-12 layered silicate nanocomposite. *J Rheol* 49(2):425–440. doi:10.1122/1.1859791
- Ayyer RK, Leonov AI (2004) Comparative rheological studies of polyamide-6 and its low loaded nanocomposite based on layered silicates. *Rheol Acta* 43(3):283–292. doi:10.1007/s00397-003-0343-6
- Bhattacharya S, Gupta R, Kamal M (2007) *Polymeric nanocomposites: theory and practice*. Hanser Gardner Publications
- Champagne MF, Huneault MA, Roux C, Peyrel W (1999) Reactive compatibilization of polypropylene polyethylene terephthalate blends. *Polym Eng Sci* 39(6):976–984. doi:10.1002/pen.11487
- Cui L, Dirniti MKB, Christopher WBB, Hunter DL, Yoon PJ, Paul DR (2008) Effect of organoclay purity and degradation on nanocomposite performance, part 1: surfactant degradation. *Polymer* 49(17):3751–3761. doi:10.1016/j.polymer.2008.06.029
- Davis CH, Mathias LJ, Gilman JW, Schiraldi DA, Shields JR, Trulove P, Sutto TE, Delong HC (2002) Effects of melt-processing conditions on the quality of poly(ethylene terephthalate) montmorillonite clay nanocomposites. *J Polym Sci B Polym Phys* 40(23):2661–2666. doi:10.1002/polb.10331
- Delozier DM, Orwoll RA, Cahoon JF, Ladislav JS, Smith JG, Connell JW (2003) Polyimide nanocomposites prepared from high-temperature, reduced charge organoclays. *Polymer* 44(8):2231–2241. doi:10.1016/s0032-3861(03)00082-x
- Dykes L, Torkelson J, Burghardt W (2012) Shear-induced orientation in well-exfoliated polystyrene/clay nanocomposites. *Macromolecules* 45(3):1622–1630
- Eslami H, Grmela M, Bousmina M (2010) Linear and nonlinear rheology of polymer/layered silicate nanocomposites. *J Rheol* 54(3):539–562. doi:10.1122/1.3372720
- Fornes TD, Paul DR (2003) Modeling properties of nylon 6/clay nanocomposites using composite theories. *Polymer* 44(17):4993–5013. doi:10.1016/s0032-3861(03)00471-3
- Fornes TD, Yoon PJ, Paul DR (2003) Polymer matrix degradation and color formation in melt processed nylon 6/clay nanocomposites. *Polymer* 44(24):7545–7556. doi:10.1016/j.polymer.2003.09.034
- Fox B, Moad G, vanDiepen G, Willing I, Cook WD (1997) Characterization of poly(ethylene terephthalate) and poly(ethylene terephthalate) blends. *Polymer* 38(12):3035–3043. doi:10.1016/s0032-3861(96)00872-5
- Frounchi M, Dourbash A (2009) Oxygen barrier properties of poly(ethylene terephthalate) nanocomposite films. *Macromol Mater Eng* 294(1):68–74. doi:10.1002/mame.200800238
- Gahleitner M, Kretschmar B, Van Vliet G, Devaux J, Pospiech D, Bernreitner K, Ingolic E (2006) Rheology/morphology interactions in polypropylene/polyamide-6 nanocomposites. *Rheol Acta* 45(322–330). doi:10.1007/s00397-005-0059-3
- Galgali G, Ramesh C, Lele A (2001) A rheological study on the kinetics of hybrid formation in polypropylene nanocomposites. *Macromolecules* 34(4):852–858. doi:10.1021/ma000565f
- Galindo-Rosales FJ, Moldenaers P, Vermant J (2011) Assessment of the dispersion quality in polymer nanocomposites by rheological methods. *Macromol Mater Eng* 296(3–4):331–340. doi:10.1002/mame.201000345
- Ghanbari A, Heuzey M, Carreau P, Ton-That MT (2012) Morphology and properties of polymer organoclay nanocomposites based on PET and sulfopolyester blends. *Polym Int*. doi:10.1002/pi.4331
- Ghasemi H, Carreau PJ, Kamal MR, Chapleau N (2011a) Effect of processing conditions on properties of pet/clay nanocomposite films. *Int Polym Process* 26(2):219–228. doi:10.3139/217.2446
- Ghasemi H, Carreau PJ, Kamal MR, Uribe-Calderon J (2011b) Preparation and characterization of PET/clay nanocomposites by melt compounding. *Polym Eng Sci* 51(6):1178–1187. doi:10.1002/pen.21874
- Ghasemi H, Carreau PJ, Kamal MR, Tabatabaei SH (2012) Properties of PET/clay nanocomposite films. *Polym Eng Sci* 52(2):420–430. doi:10.1002/pen.22099

- Gupta RK, Kennel E, Kim K-J (2009) Polymer nanocomposites handbook, 1st edn. CRC Press. Hardcover: 566 pp, ISBN-10: 0849397774, ISBN-13: 978-0849397776, 20 July 2009
- Hyun YH, Lim ST, Choi HJ, Jhon MS (2001) Rheology of poly(ethylene oxide)/organoclay nanocomposites. *Macromolecules* 34(23):8084–8093. doi:10.1021/ma002191w
- Khalkhal F, Carreau PJ (2011) Scaling behavior of the elastic properties of non-dilute MWCNT-epoxy suspensions. *Rheol Acta* 50(9–10):717–728. doi:10.1007/s00397-010-0527-9
- Khalkhal F, Carreau PJ, Ausias G (2011) Effect of flow history on linear viscoelastic properties and the evolution of the structure of multiwalled carbon nanotube suspensions in an epoxy. *J Rheol* 55(1):153–175. doi:10.1122/1.3523628
- Lim YT, Park OO (2001) Phase morphology and rheological behavior of polymer/layered silicate nanocomposites. *Rheol Acta* 40(3):220–229. doi:10.1007/s003970000126
- Litchfield D, Baird D (2006) The rheology of high aspect ratio nanoparticle filled liquids. *Rheol Rev*:1–60
- Litchfield DW, Baird DG, Rim PB, Chen C (2010) Improved mechanical properties of poly(ethylene terephthalate) nanocomposite fibers, vol 50, pp 2205–2215
- Luo ZP, Koo JH (2007) Quantifying the dispersion of mixture microstructures. *J Microsc-Oxford* 225(2):118–125. doi:10.1111/j.1365-2818.2007.01722.x
- Luo ZP, Koo JH (2008) Quantification of the layer dispersion degree in polymer layered silicate nanocomposites by transmission electron microscopy. *Polymer* 49(7):1841–1852. doi:10.1016/j.polymer.2008.02.028
- Manitiu M, Horsch S, Gulari E, Kannan RM (2009) Role of polymer-clay interactions and nano-clay dispersion on the viscoelastic response of supercritical CO₂ dispersed polyvinylmethylether (PVME)-Clay nanocomposites. *Polymer* 50(15):3786–3796. doi:10.1016/j.polymer.2009.05.036
- Mitchell CA, Krishnamoorti R (2002) Rheological properties of diblock copolymer/layered silicate nanocomposites. *J Polym Sci B Polym Phys* 40(14):1434–1443. doi:10.1002/polb.10209
- Mittal V (2011) Thermally stable and flame retardant polymer nanocomposites, 1st edn. Cambridge University Press
- Mobuchon C, Carreau PJ, Heuzey MC (2007) Effect of flow history on the structure of a non-polar polymer/clay nanocomposite model system. *Rheol Acta* 46(8):1045–1056. doi:10.1007/s00397-007-0188-5
- Mobuchon C, Carreau PJ, Heuzey MC (2009a) Structural analysis of non-aqueous layered silicate suspensions subjected to shear flow. *J Rheol* 53(5):1025–1048. doi:10.1122/1.3193720
- Mobuchon C, Carreau PJ, Heuzey MC, Reddy NK, Vermant J (2009b) Anisotropy of nonaqueous layered silicate suspensions subjected to shear flow. *J Rheol* 53(3):517–538. doi:10.1122/1.3094911
- Nazockdast E, Nazockdast H, Goharpey F (2008) Linear and nonlinear melt-state viscoelastic properties of polypropylene/organoclay nanocomposites. *Polym Eng Sci* 48(7):1240–1249. doi:10.1002/pen.21054
- Pavlidou S, Papispyrides C (2008) A review on polymer-layered silicate nanocomposites. *Prog Polym Sci* 33(12):1119–1198. doi:10.1016/j.progpolymsci.2008.07.008
- Pogodina NV, Cercle C, Averous L, Thomann R, Bouquey M, Muller R (2008) Processing and characterization of biodegradable polymer nanocomposites: detection of dispersion state. *Rheol Acta* 47(5–6):543–553. doi:10.1007/s00397-007-0243-2
- Pujari S, Dougherty L, Mobuchon C, Carreau PJ, Heuzey MC, Burghardt WR (2011) X-ray scattering measurements of particle orientation in a sheared polymer/clay dispersion. *Rheol Acta* 50(1):3–16. doi:10.1007/s00397-010-0492-3
- Ray SS, Bousmina M (2005) Poly(butylene succinate-co-adipate)/montmorillonite nanocomposites: effect of organic modifier miscibility on structure, properties, and viscoelasticity. *Polymer* 46(26):12430–12439. doi:10.1016/j.polymer.2005.10.102
- Ray SS, Okamoto M (2003). *Prog Polym Sci* 28(11):1539–1641. doi:10.1016/j.progpolymsci.2003.08.002
- Ren JX, Silva AS, Krishnamoorti R (2000) Linear viscoelasticity of disordered polystyrene-polyisoprene block copolymer based layered-silicate nanocomposites. *Macromolecules* 33(10):3739–3746. doi:10.1021/ma992091u
- Sanchez-Solis A, Romero-Ibarra I, Estrada MR, Calderas F, Manero O (2004) Mechanical and rheological studies on polyethylene terephthalate-montmorillonite nanocomposites. *Polym Eng Sci* 44(6):1094–1102. doi:10.1002/pen.20102
- Scaffaro R, Botta L, Ceraulo M, La Mantia FP (2011) Effect of kind and content of organo-modified clay on properties of PET nanocomposites. *J Appl Polym Sci* 122(1):384–392. doi:10.1002/app.34087
- Solomon MJ, Almusallam AS, Seefeldt KF, Somwangthanoj A, Varadan P (2001) Rheology of polypropylene/clay hybrid materials. *Macromolecules* 34(6):1864–1872. doi:10.1021/ma001122e
- Soon KH, Harkin-Jones E, Rajeev RS, Menary G, McNally T, Martin PJ, Armstrong C (2009) Characterisation of melt-processed poly(ethylene terephthalate)/synthetic mica nanocomposite sheet and its biaxial deformation behaviour. *Polym Int* 58(10):1134–1141. doi:10.1002/pi.2641
- Stoeffler K, Lafleur PG, Denault J (2008) Thermal decomposition of various alkyl onium organoclays: effect on polyethylene terephthalate nanocomposites' properties. *Polym Degrad Stab* 93(7):1332–1350. doi:10.1016/j.polymdegradstab.2008.03.029
- Sun L, Boo WJ, Liu J, Clearfield A, Sue HJ, Verghese NE, Pham HQ, Bicerano J (2009) Effect of nanoplatelets on the rheological behavior of epoxy monomers. *Macromol Mater Eng* 294(2):103–113. doi:10.1002/mame.200800258
- Todorov LV, Viana JC (2007) Characterization of PET nanocomposites produced by different melt-based production methods. *J Appl Polym Sci* 106(3):1659–1669. doi:10.1002/app.26716
- Utracki LA, Lyngaae-Jorgensen J (2002) Dynamic melt flow of nanocomposites based on poly-epsilon-caprolactam. *Rheol Acta* 41(5):394–407. doi:10.1007/s003970100211
- Van Krevelen D, Te Nijenhuis K (2009) Properties of polymers, 4th edn. Elsevier Science. 1032 pp, ISBN: 9780080548197
- Vermant J, Ceccia S, Dolgovskij MK, Maffettone PL, Macosko CW (2007) Quantifying dispersion of layered nanocomposites via melt rheology. *J Rheol* 51(3):429–450. doi:10.1122/1.2516399
- Wan T, Wang B, Liao S, Clifford M (2012) Rheological investigation on the interaction of polyamide 6 with clay. *J Appl Polym Sci* 125:E27–E33. doi:10.1002/app.35554
- Wang BA, Wan T, Zeng W (2011) Dynamic rheology and morphology of polylactide/organic montmorillonite nanocomposites. *J Appl Polym Sci* 121(2):1032–1039. doi:10.1002/app.33717
- Wu DF, Zhou CX, Hong Z, Mao DL, Bian Z (2005) Study on rheological behaviour of poly(butylene terephthalate)/montmorillonite nanocomposites. *Eur Polym J* 41(9):2199–2207. doi:10.1016/j.eurpolymj.2005.03.005
- Xia HS, Song M (2006) Intercalation and exfoliation behaviour of clay layers in branched polyol and polyurethane/clay nanocomposites. *Polym Int* 55(2):229–235. doi:10.1002/pi.1948
- Xu X, Ghanbari A, Leelapornpisit W, Heuzey M, Carreau P (2011) Effect of Ionomer on barrier and mechanical properties of PET/organoclay nanocomposites prepared by melt compounding. *Int Polym Process* 26(4):444–455. doi:10.3139/217.2477
- Yoon PJ, Hunter DL, Paul DR (2003) Polycarbonate nanocomposites: part 2. Degradation and color formation. *Polymer* 44(18):5341–5354. doi:10.1016/s0032-3861(03)00523-8
- Yziquel F, Carreau PJ, Tanguy PA (1999) Non-linear viscoelastic behavior of fumed silica suspensions. *Rheol Acta* 38(1):14–25. doi:10.1007/s003970050152